CORA Cork Open Research Archive
Cartlann Taighde Oscailte Chorcaí

Title	Activation of CO2 at chromia-nanocluster-modified rutile and anatase TiO2
Authors	Nolan, Michael;Fronzi, Marco
Publication date	2018-11-27
Original Citation	Nolan, M. and Fronzi, M. (2018) 'Activation of CO2 at chromia-nanocluster-modified rutile and anatase TiO2', Catalysis Today. doi:10.1016/j.cattod.2018.11.062
Type of publication	Article (peer-reviewed)
Link to publisher's version	10.1016/j.cattod.2018.11.062
Rights	© 2018, Elsevier B.V. All rights reserved. This manuscript version is made available under the CC-BY-NC-ND 4.0 license. - https://creativecommons.org/licenses/by-nc-nd/4.0/
Download date	2026-11-17 10:57:25
Item downloaded from	https://hdl.handle.net/10468/7162



UCC
University College Cork, Ireland
Coláiste na hOllscoile Corcaigh

Supporting Information for

Activation of CO_2 at Chromia-Nanocluster-Modified Rutile and Anatase TiO_2

Michael Nolan[1]* and Marco Fronzi[1,2]

1: Tyndall National Institute, University College Cork, Lee Maltings, Prospect Row, Cork, T12 R5CP, Ireland

2: International Research Centre for Renewable Energy, State Key Laboratory of Multiphase Flow in Power Engineering, Xi'an Jiaotong University, Xi'an 710049, Shaanxi, China.

*michael.nolan@tyndall.ie

This supporting information document contains the following

1. Given the length restrictions in a Catalysis Today submission, we provide full detailed description of the methods used in the paper

2. Figure S1 shows the atomic structure of chromia nanocluster modified oxidised rutile (110) and anatase (101) and hydroxylated rutile (110) and anatase (101)

3. Figure S2 shows the atomic structure of reduced chromia nanocluster modified oxidised rutile (110) and anatase (101) and hydroxylated rutile (110) and anatase (101) in which an oxygen vacancy is present in the chromia nanocluster.

4. Figure S3 shows the atomic structure of different CO_2 adsorption modes on chromia-modified oxidised rutile (a)-(c) and chromia-modified hydroxylated rutile (d)-(f)

5. Figure S4 shows the atomic structure of different CO_2 adsorption modes on chromia-modified oxidised anatase (a)-(c) and chromia-modified hydroxylated anatase (d)-(f)

6. Table S1 shows relative energies of different CO_2 adsorption modes where the most stable adsorption mode is set to 0 eV.

Methods

We use the computational approach from our previous work on chromia-modified rutile and anatase[1] and prepare heterostructures composed of rutile (110) and anatase (101) modified with Cr_4O_6 nanoclusters. The main text discusses how we prepare chromia-modified rutile and anatase.

We use a three dimensional periodic surface slab within the VASP code [2-5], and a plane wave basis set to describe the valence electrons. Projector augmented wave potentials [6, 7], with 4, 12, 6, 4 and 1 valence electrons for Ti, Cr, O, C and H describe the core-valence electron interactions. This set-up was tested in our earlier publication on Cr_2O_3-modified TiO_2[1]. The cut-off for the kinetic energy is 396 eV and the exchange-correlation functional is the Perdew-Wang 91 [8] approximation. A Monkhorst-Pack (2×1×1) k-point sampling grid is used.

For consistency with our previous work we apply the DFT+U approach [9] to describe the Ti 3d and Cr 3d states. A well accepted standard value of U = 4.5 eV is applied for Ti 3d states and we apply a typical value of 3.5 eV for Cr 3d states [10, 11]. The convergence criteria for the electronic and ionic relaxations are 0.0001 eV and 0.02 eV/ Å. Methfessel-Paxton smearing is used with σ = 0.1 eV (used also for broadening of the peaks in the electronic density of states). All calculations are spin polarised throughout, with no constraints on the spin.

The perfect rutile (110) surface is terminated by two-fold coordinated bridging O atoms, with 3-fold coordinated in-plane oxygen atoms in the surface layer. In the same layer, the Ti atoms take 5-fold and 6-fold coordination, with the latter bonded to the two-fold coordinating bridging oxygen atoms.

The perfect anatase (101) surface is characterised by two-fold coordinated oxygen atoms terminating the surface layer and the outermost Ti atoms are 5-fold coordinated.

The effect of surface water is modelled by a decorating the rutile and anatase surfaces with ½ ML of dissociated water forming surface bound hydroxyl groups. This set-up has been used in previous work [1, 12]

(2x4) and (4x2) surface supercell expansions are employed for rutile (110) and anatase (101), respectively and the vacuum gap in all cases is 12 Å.

In forming the composite structures, we relax the chromia nanocluster in a large supercell to model an isolated gas phase nanocluster. The oxide nanocluster modifier is adsorbed at different TiO_2 surfaces in different configurations and these are relaxed [13-15]. The most stable Cr_2O_3-TiO_2 composites from ref. [1] are then used for the study of CO_2 activation in the present paper.

The stability of the heterostructure is characterised by the computed nanocluster adsorption energy, E^{ads}

$$E^{ads} = E[(Cr_4O_6)\text{-}TiO_2] - \{E[Cr_4O_6] + E[TiO_2]\}6 \qquad (1)$$

Where $E[(Cr_4O_6\text{-}TiO_2]$ is the computed total energy of the Cr_4O_6 nanocluster-modified TiO_2 surface, $E(Cr_4O_6)$ is the computed total energy of the free Cr_4O_6 nanocluster and $E(TiO_2)$ is the computed total energy of the unmodified TiO_2 (rutile/anatase) surface. This energy can be considered to determine how resistant the nanocluster is to desorption after it has been deposited onto the TiO_2; the deposition could be by atomic layer deposition or incipient wetness impregnation.

The CO_2 adsorption energy is defined in Eqn (2):

$$E^{ads} = E(CO_2@Cr_4O_6\text{-}TiO_2) - \{E(Cr_4O_6\text{-}TiO_2) + E(CO_2)\} \qquad (2)$$

where $E(CO_2@Cr_4O_6\text{-}TiO_2)$ is the computed total energy of CO_2 adsorbed at Cr_4O_6-modified TiO_2. While van de Waals corrections can be added, the change in the computed adsorption energies is *ca*. 0.15 eV, which is insignificant compared to the magnitude of the CO_2 adsorption energies. We examined many CO_2 adsorption structures and those shown in the main text are the most stable that we have found. We also show in Figures S3 and S4 other CO_2 adsorption modes that are less stable than those described in the main text.

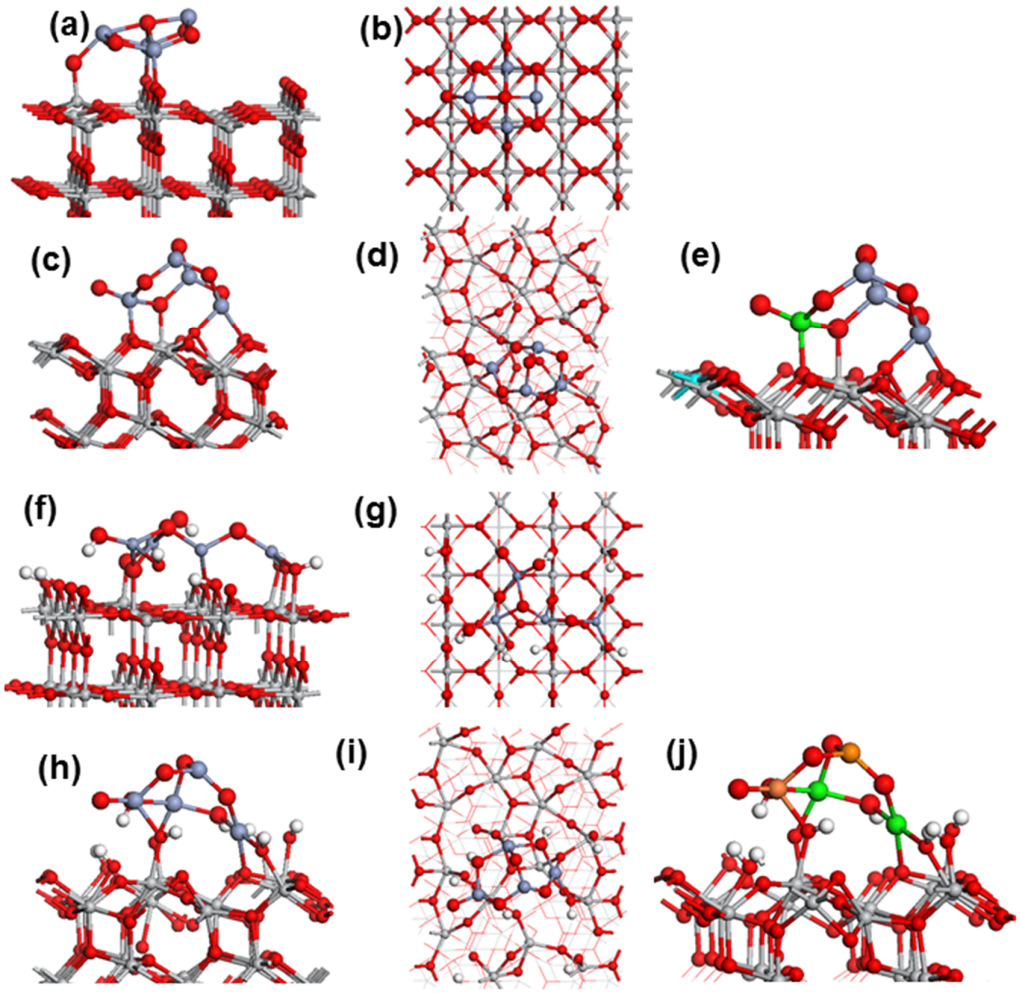


Figure S1: Atomic structure of a Cr_4O_6 nanocluster adsorbed on **(a), (b)** rutile (110), **(c)-(e)** TiO_2 anatase (101), **(f), (g)** 1/2ML hydroxyls on rutile (110) and **(h)-(j)** ½ ML hydroxyls on anatase (101). Reduced Ti^{3+}, reduced Cr^{2+} and oxidised Cr^{4+} species are coloured cyan, orange and green.

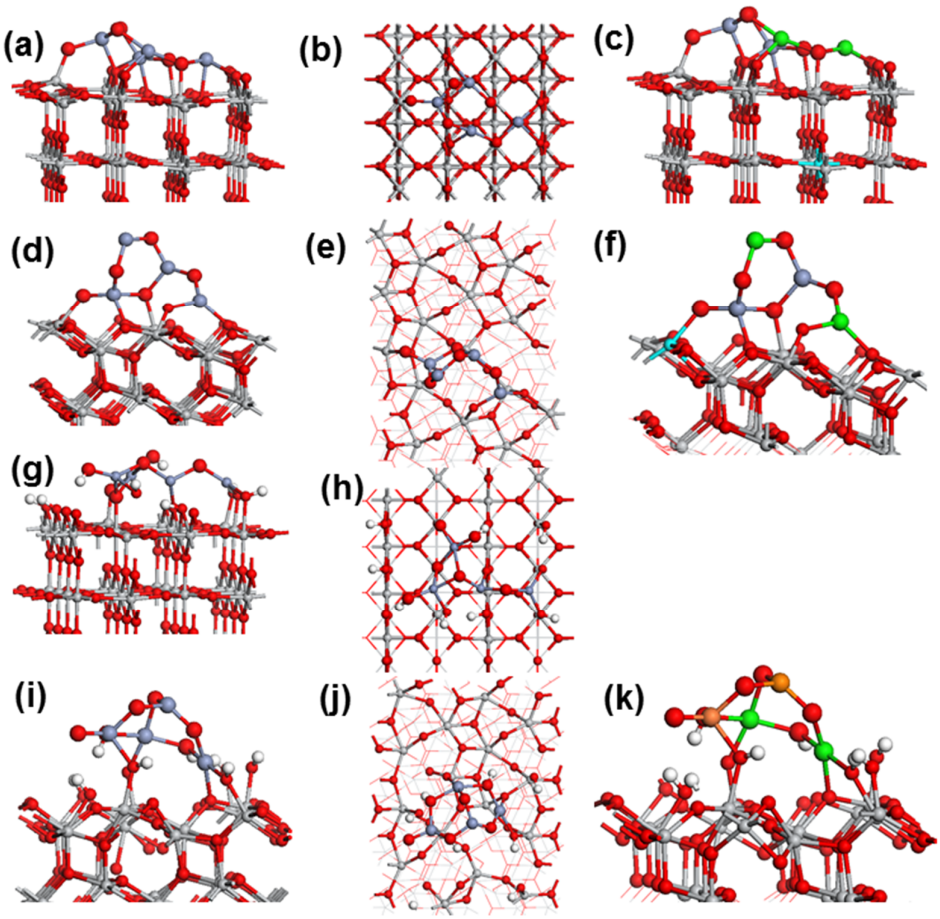


Figure S2: Atomic structure of the most stable reducing oxygen vacancy in Cr_4O_6 nanocluster modified TiO_2. **(a) - (c)** rutile (110), **(d)-(f)** anatase (101), **(g), (h)** 1/2ML hydroxyls on rutile (110) and **(i)-(k)** ½ ML hydroxyls on anatase (101). Reduced Ti^{3+}, reduced Cr^{2+} and oxidised Cr^{4+} species are coloured cyan, orange and green.

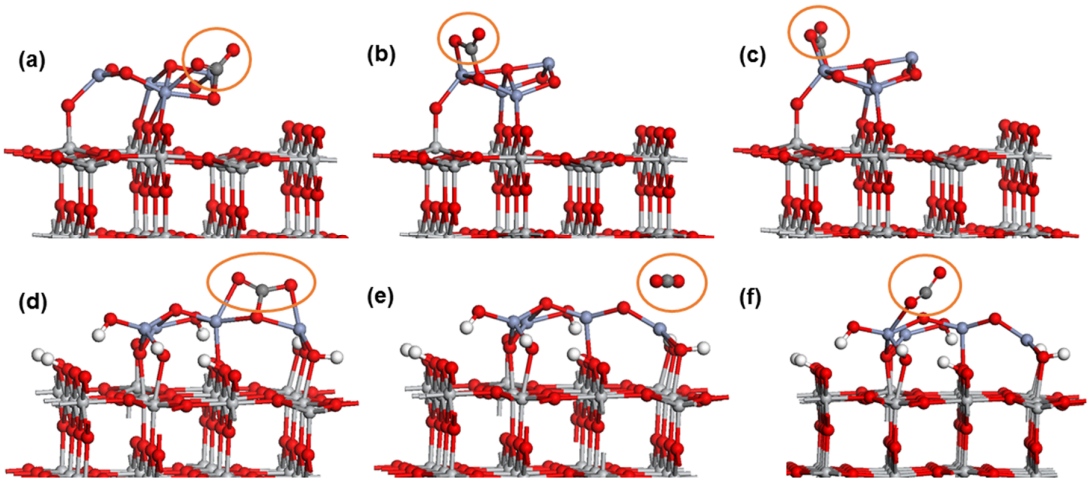


Figure S3: Higher energy CO_2 adsorption modes when adsorbed at Cr_4O_6-o-rutile (110) and Cr_4O_6-oh-rutile (110). The energy relative to the most stable structure in the main text is also shown.

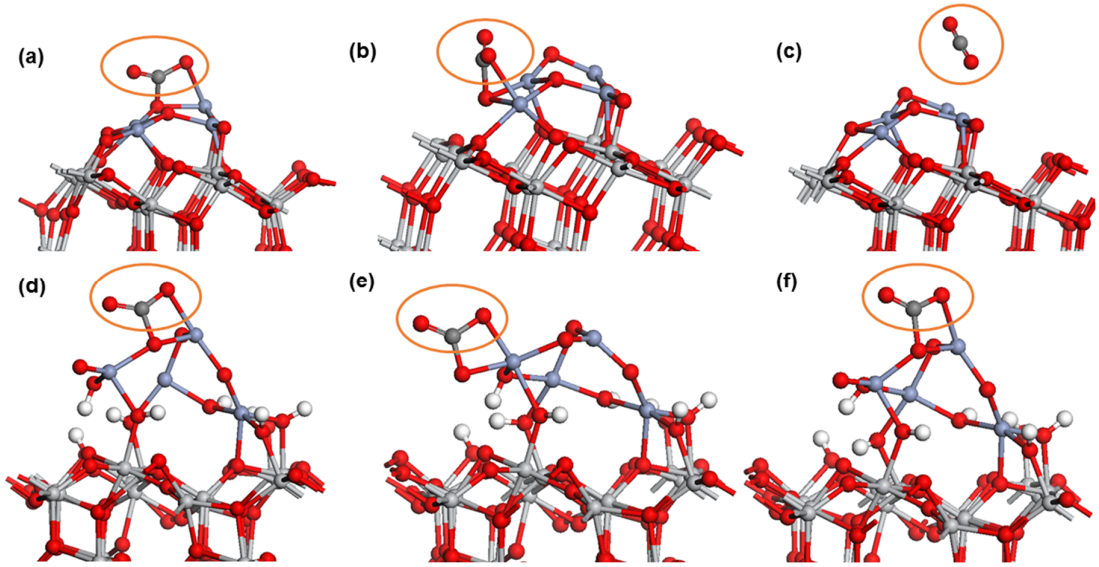


Figure S4: Higher energy CO_2 adsorption modes when adsorbed at Cr_4O_6-o-anatase (101) and Cr_4O_6-oh-anatase (101).

Table S1 shows the energies of the CO_2 adsorption modes on chromia-modified rutile and chromia-modified anatase relative to the most stable adsorption modes shown in the main text. The energy of the most stable adsorption mode is set to 0 eV

Cr_4O_6-o-rutile	
Adsorption mode	**$E^{relative}$ / eV**
Figure 1(a)	0.28
Figure 1(b)	**0.0**
Figure S3 (a)	0.40
Figure S3(b)	0.11
Figure S3 (c)	0.10
Cr_4O_6-oh-rutile	
Adsorption mode	**$E^{relative}$ / eV**
Figure 1(c)	**0.0**
Figure 1(d)	0.61
Figure S3 (a)	0.68
Figure S3(b)	0.62
Figure S3 (c)	0.60
Cr_4O_6-o-anatase	
Adsorption mode	**$E^{relative}$ / eV**
Figure 2(a)	**0**
Figure 2(b)	Forms CO
Figure S3 (a)	0.40
Figure S3(b)	0.45
Figure S3 (c)	0.31
Cr_4O_6-oh-anatase	
Adsorption mode	**$E^{relative}$ / eV**
Figure 2(c)	0.40
Figure 2(d)	**0**
Figure S3 (a)	1.10
Figure S3(b)	0.45
Figure S3 (c)	1.01

Table S1: Energies of CO_2 adsorption modes on chromia-modified rutile and chromia-modified anatase relative to the most stable adsorption mode described in the main text. The energy of this adsorption mode is set to 0 eV

References

[1] M. Fronzi, M. Nolan, Surface Modification of Perfect and Hydroxylated TiO_2 Rutile (110) and Anatase (101) with Chromium Oxide Nanoclusters, ACS Omega, 2 (2017) 6795-6808.
[2] G. Kresse, J. Hafner, Ab initio molecular dynamics for liquid metals, Phys. Rev. B., 47 (1993) 558.
[3] G. Kresse, J. Hafner, *Ab initio* molecular-dynamics simulation of the liquid-metal-amorphous-semiconductor transition in germanium, Phys. Rev. B., 49 (1994) 14251-14269.
[4] G. Kresse, J. Furthmüller, Efficiency of Ab-initio Total Energy Calculations for Metals and Semiconductors using a Plane-wave Basis Set, Computational Materials Science, 6 (1996) 15-50.
[5] G. Kresse, J. Furthmüller, Efficient Iterative Schemes for Ab-initio Total-energy Calculations using a Plane-wave Basis Set, Phys. Rev. B., 54 (1996) 11169.
[6] G. Kresse, D. Joubert, From ultrasoft pseudopotentials to the projector augmented-wave method, Phys. Rev. B., 59 (1999) 1758-1775.
[7] P.E. Blöchl, Projector augmented-wave method, Phys. Rev. B., 50 (1994) 17953-17979.
[8] J.P. Perdew, J.A. Chevary, S.H. Vosko, K.A. Jackson, M.R. Pederson, D.J. Singh, C. Fiolhais, Atoms, molecules, solids, and surfaces: Applications of the generalized gradient approximation for exchange and correlation, Phys. Rev. B., 46 (1992) 6671-6687.
[9] S. Dudarev, G. Botton, S. Savrasov, C. Humphreys, A. Sutton, Electron-Energy-Loss Spectra and the Structural Stability of Nickel Oxide: An LSDA+U study, Phys. Rev. B., 57 (1998) 1505.
[10] J.J. Carey, M. Nolan, Enhancing the oxygen vacancy formation and migration in bulk chromium(III) oxide by alkali metal doping: a change from isotropic to anisotropic oxygen diffusion, J. Mater. Chem. A, 5, (2017), 15163.
[11] J.J. Carey, M. Legesse, M. Nolan, Low Valence Cation Doping of Bulk Cr_2O_3: Charge Compensation and Oxygen Vacancy Formation, J. Phys. Chem. C, 120 (2016) 19160-19174.
[12] M. Fronzi, A. Iwaszuk, A. Lucid, M. Nolan, Metal oxide nanocluster-modified TiO_2 as solar activated photocatalyst materials, J. Phys.: Condens. Matter, 28 (2016) 074006.
[13] A. Iwaszuk, M. Nolan, Reactivity of sub 1 nm supported clusters: $(TiO_2)_n$ clusters supported on rutile TiO_2 (110), Phys. Chem. Chem. Phys., 13 (2011) 4963-4973.
[14] A. Lucid, A. Iwaszuk, M. Nolan, A first principles investigation of Bi_2O_3-modified TiO_2 for visible light Activated photocatalysis: The role of TiO_2 crystal form and the Bi^{3+} stereochemical lone pair, Mater. Sci. Semicond. Process., 25 (2014) 59-67.
[15] M. Nolan, A. Iwaszuk, A.K. Lucid, J.J. Carey, M. Fronzi, Design of novel visible light active photocatalyst materials: surface modified TiO_2, Adv. Mater., 28 (2016) 5425-5446.